

TV White Space Regulated Broadband Power Line Communication for Point-to-Multipoint Downlink IoT Networks: A Standard Perspective

Mohammad Heggo^{ID}, Member, IEEE, Sumei Sun^{ID}, Fellow, IEEE, Xu Zhu^{ID}, Senior Member, IEEE, and Yi Huang^{ID}, Senior Member, IEEE

Abstract—Broadband power line communication (BPLC) and television white space (TVWS) are regarded as promising candidates for indoor broadband applications of the Internet of Things. However, they share the access to the very high frequency (VHF) band, which could cause harmful interference and performance degradation to each other. In this paper, a TVWS regulated BPLC system is proposed for point-to-multipoint downlink communication, which integrates the requirement of primary user sensing and the permissible transmission power spectral density (PSD) for TVWS users into the BPLC standard, regarding VHF band access. This integration guarantees minimum interference level between TVWS and BPLC and allows higher transmission PSD for BPLC users in VHF, and hence higher capacity and coverage for BPLC.

Index Terms—Broadband communications, cognitive radio, design standards, indoor communications, Internet of Things (IoT), MIMO.

I. INTRODUCTION

THE revolutionary development in communication technologies and protocols that took place in the last decade assists information exchange with high speed and large bandwidth. This creates a reliable backhaul network that can support Internet of Things (IoT) services, which encompass connecting different objects and sensors with different communication technologies into one network [1], [2]. Television white space (TVWS) communication and broadband power line communication (BPLC) are two promising technologies that introduce cost-effective solutions for high speed

Manuscript received July 15, 2018; revised October 4, 2018; accepted October 8, 2018. Date of publication October 16, 2018; date of current version July 31, 2019. This work was supported in part by Innovate UK under the Liverpool5G project, the University of Liverpool, and the Science and Technology Innovation Commission of Shenzhen under Project No. JCYJ20170307151258279. (Corresponding author: Xu Zhu.)

M. Heggo is with the Department of Electrical Engineering and Electronics, University of Liverpool, Liverpool L69 3GJ, U.K., and also with the Institute for Infocomm Research (I2R), Agency for Science, Technology, and Research, Singapore (e-mail: m.heggo@liverpool.ac.uk).

S. Sun is with the Institute for Infocomm Research (I2R), Agency for Science, Technology, and Research, Singapore (e-mail: sunsm@i2r.a-star.edu.sg).

X. Zhu is with the Department of Electrical Engineering and Electronics, University of Liverpool, Liverpool L69 3GJ, U.K., and also with the School of Electronic and Information Engineering, Harbin Institute of Technology, Shenzhen 518052, China (e-mail: xuzhu@liverpool.ac.uk).

Y. Huang is with the Department of Electrical Engineering and Electronics, University of Liverpool, Liverpool L69 3GJ, U.K. (e-mail: huangyi@liverpool.ac.uk).

Digital Object Identifier 10.1109/JIOT.2018.2876415

applications, especially in the indoor environment [3]–[6]. The two technologies have been recently introduced to support machine-to-machine services in IoT network [7]–[9]. However, TVWS and BPLC share the very high frequency (VHF) band, which can introduce potential interference if they are integrated into the same IoT network. This interference can affect the achievable throughput and coverage distance, which drives our need for deeper study into the regulatory standards of both technologies to achieve better cooperation and integration into an IoT network.

Cognitive access of TVWS spectrum was recommended by the federal communication commission (FCC) in May 2004 [10]. In December 2008, FCC issued the second report [11] to regulate TVWS cognitive communication. The report regulates the transmission power limits over the secondary users (SUs) in order to protect the primary users (PUs) from interference. SUs shall acquire sufficient information about PU activity before utilizing the TV channel. Hence, the SU shall be connected to a geolocation database and/or have high sensing capabilities. The geolocation database has a detailed temporal and geographical map for the availability of PU TV channels.

BPLC has drawn researchers' attention in last decade as a promising technology for high speed indoor applications. However, power line cables have not been designed or shielded to carry the communication signals, which causes communication signal power loss due to electromagnetic radiation [12], [13]. This radiation can cause severe interference to surrounding wireless services, which share the same band in particular, TV and radio wireless services in the VHF band [14]–[16]. Consequently, the electromagnetic compatibility regulations limit the power spectral density (PSD) of BPLC transmitter to avoid interference with existing wireless services. For example, the standard of the comité Européen de normalisation électrotechnique [6] limits the PSD of BPLC signal to -55 dBm/Hz in the high frequency (HF) band between 1.8 and 30 MHz, and -80 dBm/Hz in the VHF band between 30 and 100 MHz. The 25 dB difference in the allowed PSD between the HF and the VHF band yields a significant degradation in BPLC achievable throughput and coverage distance in VHF band compared to HF band. In [17] and [18], the cooperation was proposed between TVWS and BPLC point-to-point systems in VHF band only from both throughput

and regulations perspectives, while an overall TVWS BPLC standard framework for both HF and VHF bands was not considered. Also, the coverage and throughput analysis of the downlink point-to-multipoint TVWS BPLC communication were not addressed.

In this paper, to mitigate the interference challenge in realizing an IoT network, we propose a standard framework which integrates the HomeplugAV2 standard [6], [14] for BPLC and the ECMA-392 standard [19] for TVWS into a point-to-multipoint communication system, which is referred to as high throughput white BPLC (HT-WBPLC). This paper is different from the previous work in the following aspects.

- 1) To the best of our knowledge, this is the first work to investigate the integration of BPLC with TVWS in a downlink point-to-multipoint communication system, which integrates the requirement of PU sensing and the permissible transmission PSD for TVWS users into the BPLC standard. Based on standard compatibility and our channel measurement results, the proposed standard framework enables additional frequency band of 100–200 MHz to be used by BPLC, guarantees minimum interference level between TVWS and BPLC and allows higher transmission PSD for BPLC users in VHF. Both coverage and throughput analysis are provided for the proposed HT-WBPLC system. The results obtained show the benefit of utilizing the crosstalk between wireless TVWS and BPLC to enhance the overall HT-WBPLC system performance, especially in the frequency beyond 100 MHz. HT-WBPLC achieves higher throughput and coverage compared to MIMO BPLC.
- 2) The proposed HT-WBPLC standard framework allows three point-to-multipoint operating modes: a) BPLC in HF; b) TVWS in VHF and in PU absence; and c) BPLC in VHF and in PU presence, according to PU status and operating frequency band, leading to a higher degree of freedom in adapting to different standard requirements of BPLC and TVWS. Resource allocation for the proposed HT-WBPLC standard framework is investigated to maximize the system throughput under different requirements of operating modes, while the previous work on resource allocation for orthogonal frequency division multiple access-based cognitive radio networks [20]–[25] cannot be applied directly, as each operating mode has their specific PSD and subchannel frequency spacing.

The rest of this paper is organized as follows. In Section II, we present the proposed HT-WBPLC system model for IoT network. In Section III, channel measurement results for the cross-talk between wireless TVWS channel and BPLC channel are presented. In Section IV, frequency and power allocation problem for different users is investigated and optimal solution is proposed. In Section V, point-to-multipoint system simulation results are presented to evaluate the performance of our proposed HT-WBPLC system and in comparison to TVWS and MIMO BPLC systems. In Section VI, this paper is concluded.

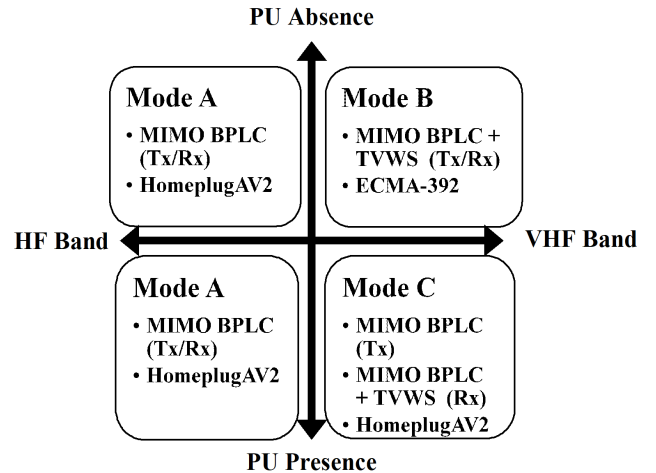


Fig. 1. HT-WBPLC modes of operation.

II. HT-WBPLC: STANDARD OVERVIEW AND SYSTEM MODEL

A. HT-WBPLC Standard for IoT Networks

The first edition of ECMA-392 [19] standard was released in 2009 for TVWS communications, and the second edition was released in 2012. Also, HomplugsAV2 standard [14] was issued in 2012 as an extension to the IEEE 1901 standard for BPLC systems. The common band between ECMA-392 and HomeplugAV2 standards is the VHF band. However, BPLC and TVWS transceivers are permitted to access the VHF band at different transmission PSD levels. BPLC transceiver uses -80 dBm/Hz PSD to access VHF band compared to -47.7 dBm/Hz PSD, in case of TVWS transceiver.

The proposed standard amendment for HT-WBPLC allows the integration of TVWS and BPLC into one communication system in IoT network. Hence, it incorporates both ECMA-392 and HomeplugAV2 standards. HT-WBPLC has three modes of operation according to the frequency band and PU activity. In Fig. 1, different operating modes of HT-WBPLC are mapped over four quadrants, where the upper part of the figure represents PU absence case and the right part represents VHF band access and vice versa. The three HT-WBPLC modes can be explained as follows.

1) *Mode A*: This mode spans the frequency band 1.8–30 MHz. Consequently, HomplugsAV2 standard is adopted for the physical (PHY) and medium access control (MAC) layers in communication with transmission signal PSD of -55 dBm/Hz. The band below 30 MHz has the advantage that it is a completely free band, which can provide a backup channel when all TVWS channels are occupied. In WBPLC, single-input single-output (SISO) BPLC is used for communication, while in the HT-WBPLC, MIMO BPLC is used.

2) *Mode B*: This mode deals with the case of the PU absence in VHF band. Therefore, the spanned frequency spectrum is 54–200 MHz. According to FCC regulations, nine TV channels are allowed for cognitive access in this band which are: 54–60 MHz, 60–66 MHz, 66–72 MHz, 76–82 MHz, 82–88 MHz, 174–180 MHz, 180–186 MHz, 186–192 MHz,

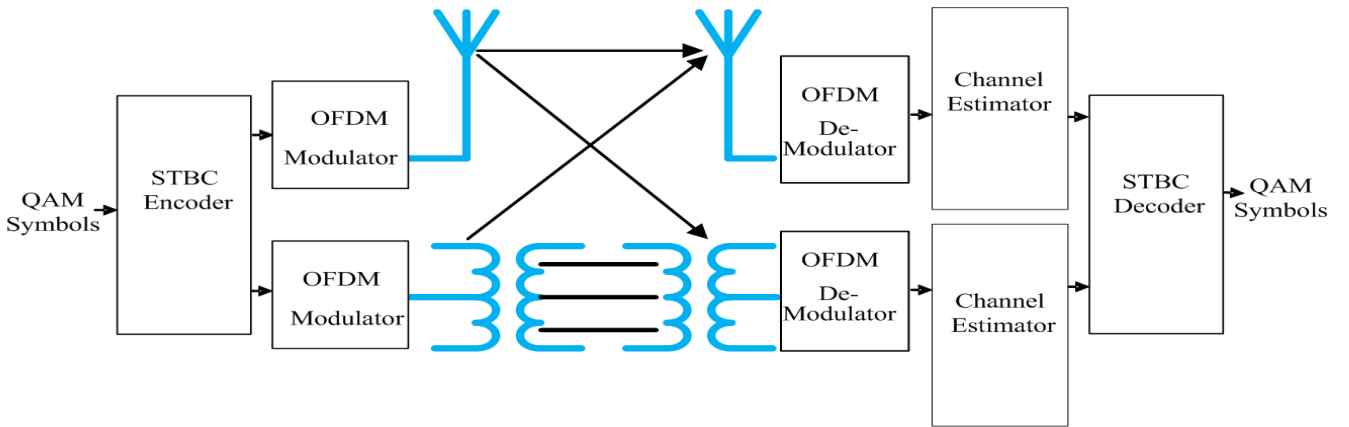


Fig. 2. Block diagram of the HT-WBPLC system.

TABLE I
HT-WBPLC MODES OF OPERATION

| | Mode A | Mode B | Mode C |
|------------------------------|------------------|-----------------------------------------------------------------|------------------|
| Frequency Band | 1.8 MHz - 30 MHz | 54 MHz - 200 MHz | 30 MHz - 200 MHz |
| Tx Type | BPLC | BPLC + TVWS | BPLC |
| Rx Type | BPLC | BPLC + TVWS | BPLC + TVWS |
| Communication Standard | HomeplugAV2 | ECMA-392 | HomeplugAV2 |
| PSD | -55 dBm/Hz | -47.7 dBm/Hz (free channel), -51.7 dBm/Hz (adjacent channel) | -80 dBm/Hz |
| Tx/Rx Ports maximum number | 2 Tx & 2 Rx | 3 Tx & 3 Rx | 2 Tx & 3 Rx |
| Number of Subcarriers | 1156 | 1152 | 1260 |
| Subcarrier frequency spacing | 24.414 kHz | 46 kHz | 46 kHz |

and 192–198 MHz. ECMA-392 standard is adopted in the PHY and MAC layers design. Consequently, the maximum allowed PSD for each 6 MHz channel is -47.7 dBm/Hz and -51.7 dBm/Hz for nonadjacent and adjacent channels, respectively. As a result, our HT-WBPLC system offers BPLC at least 34 dB increase in the PSD in VHF band, hence can significantly improve the achievable throughput. In mode B, BPLC channel is used cooperatively with the wireless TVWS channel, which increases the number of spatial channels.

3) *Mode C*: This mode deals with the case of the PU presence in VHF band. The spanned frequency band is 30–200 MHz. HomeplugAV2 standard is adopted for the PHY and MAC layers of communication. Therefore, the PSD is restricted to -80 dBm/Hz.

The main features of the three modes of HT-WBPLC operation are summarized in Table I.

B. HT-WBPLC System Model

In Fig. 2, the system model for HT-WBPLC point-to-multipoint communication system is shown. The model is

applied to the three modes of HT-WBPLC operation. The M-ary quadrature amplitude modulation (QAM) with gray bit mapping is used as a submodulation for the subcarriers in the orthogonal frequency division multiplexing (OFDM) symbol. Each QAM modulated signal is then sent to space time block coding (STBC) encoder, which transmits the same QAM symbol over both BPLC and TVWS channels. The transmission power for each OFDM subcarrier is regulated according to the proposed standard amendment in this section, while the subcarrier and power allocation problem for MIMO HT-WBPLC channel is discussed in detail in Section IV.

III. HT-WBPLC MIMO CHANNEL MODEL

A. Channel Estimation

HT-WBPLC channel estimation is subdivided into two categories: 1) PU and 2) SU channel estimation. PU channel estimation is obtained using two methods: 1) geolocation database communication and 2) carrier sensing. Each method has its own advantages and drawbacks. Geolocation database communication supports a safer mechanism for the TV band licensed users to protect their network [26], [27]. As a result, the office of communications in U.K. stated “the most important mechanism in the short to medium term will be geolocation” [27]. However, the geolocation database can suffer some prediction errors and differences from real measured PU data as stated in [28], which raises the problems of PU carrier misdetection and false alarm. Hence, sensing techniques are recommended to enhance PU carrier detection. The main challenge of PU carrier sensing is determining the accurate threshold with respect to misdetection and false alarm probabilities [26]. Determining the optimum threshold for PU carrier sensing was approached in this paper [17], where the throughput of point-to-point HT-WBPLC system was investigated compared to MIMO BPLC. In [17], an MIMO sensing algorithm was proposed for the PU signal, where probabilities of detection and false alarm of 0.99 and $1e-7$ were achieved, respectively.

Regarding SU channel estimation, feedback is assumed between HT-WBPLC Tx and Rx. The impact of channel

estimation error on the overall throughput of point-to-point HT-WBPLC system was investigated in this paper in [29].

In this paper, we focus on coverage area and throughput analysis of point-to-multipoint HT-WBPLC system compared to MIMO BPLC system in [14], ignoring the channel estimation problems for both PU and SU that had been addressed in [17] and [29]. Perfect channel state information is assumed available for SU Tx and Rx as in [23]–[25] and [30]. We rely on geolocation database communication for PU presence as recommended in [26] and [27].

B. Channel Model

BPLC indoor channel was investigated in VHF band in [31]. The path loss of BPLC was proved to be frequency selective and dependent on several factors like: power line cable type, power outlet density, power line cable branch lengths, and terminal loads. Also, VHF path loss model for indoor wireless channel was modeled in [32]. The wireless path loss depends mainly on separating geometric distance, number of separating walls and floors. Moreover, several studies in [33]–[35] suggested enhancing BPLC signal reception by adding an antenna to the receiver and hence, can compromise the radiated electric field.

In this paper, we extend the channel measurements conducted in [13] and [31], to include the crosstalk between BPLC and TVWS wireless channels. The aim of channel measurements is path loss modeling of the crosstalk channel and comparing it against BPLC channel path loss. In [13], BPLC wireless channel measurements in the frequency band 1.7–100 MHz show channel capacities of 450 and 85 Mb/s for both short and long distances, respectively. This result proves the promising application of the standard amendment proposed in this paper to regulate HT-WBPLC system. Since, HT-WBPLC is proposed to span VHF band up to 200 MHz, the frequency band of our channel measurements is 84–200 MHz. However, we avoid the frequency modulation (FM) band from 88 to 110 MHz due to the interference from FM radio. The channel measurements are held inside the laboratories and offices within the Department of Electrical Engineering and Electronics of the University of Liverpool, which makes the results applicable to indoor office environment. The Tx and Rx are located at the same floor. The channel between any two power line couplers is represented by network of power line cables, while the channel between any two wireless antennas is the radio propagation channel. The path loss is measured using radio frequency (RF) signal generator at Tx and spectrum analyzer at Rx. The path loss is measured for three different channels: 1) the channel between two power line coupling circuits, referred to as h_{11} ; 2) the channel between a coupling circuit at Tx and wireless antenna at Rx, referred to as h_{12} ; and 3) the channel between wireless antenna at Tx and power line coupling circuit at Rx, referred to as h_{21} .

Two broadband coupling circuits have been used in Tx and Rx. The coupling circuit has been designed to be broadband inductive as in [36], to achieve flat gain in broadband application. The loss has been measured in the

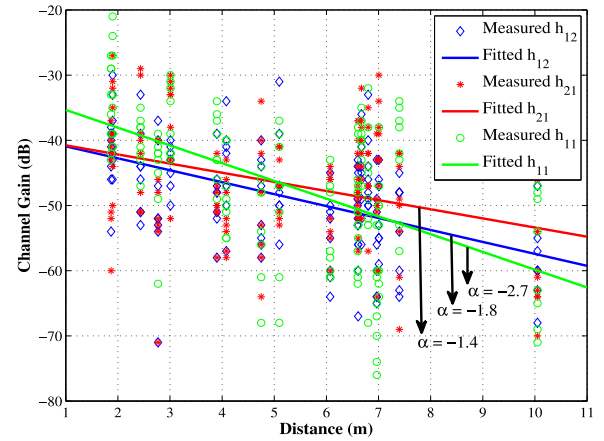


Fig. 3. Crosstalk channel compared to BPLC channel.

coupling circuits and the connection cables by measuring their S-parameters using the network analyzer for calibration purpose. The channel measurements have been carried out between the outlets belonging to the same phase and the same distribution box. The channel measurements have been done in different rooms to have an average path loss representation.

In Fig. 3, the gain of the crosstalk and BPLC channels are shown versus distance. The channel gain is measured at four frequencies in the band 84–200 MHz, which are 84 MHz, 110 MHz, 140 MHz, and 190 MHz. The gain in Fig. 3 is mapped for all aforementioned four frequencies to better describe the path loss in the whole frequency band rather than single frequency tone. The gain is measured for each frequency at different coverage distances to model the path loss of the channel. The channel measurement results show that BPLC and crosstalk channels have close gain performance with respect to distance, since the slope α of the fitted channel gain takes the values of -2.7 , -1.8 , and -1.4 for the h_{11} , h_{12} , and h_{21} , respectively. Also, the results show that the crosstalk channel gain is below BPLC channel gain for small coverage distance; however for long coverage distances the crosstalk channel gain outperforms the corresponding BPLC channel gain. This is due to the dependence of the crosstalk channel gain mainly on the geometric separation distance between Tx and Rx. However, BPLC channel gain is mainly dependent on the electric separation distance, which is the length of the power line cable connecting the Tx to the Rx. It is known that the electric distance is longer than the geometric distance as reported in [31].

An important observation can be deduced from Fig. 3, which is measured channel gain large variance about its mean value. BPLC channel gain with respect to geometric Tx–Rx distance is characterized by its large variance, as have been proved in previous literature measurements [37]. This is due to BPLC channel gain dependency on Tx–Rx “electric distance” rather than “geometric distance.” Also, BPLC channel gain varies according to powerline topology, cable connections, connected loads, and outlet density, which increases the overall channel variance about its mean value.

IV. THROUGHPUT MAXIMIZATION AND POWER ALLOCATION IN HT-WBPLC

In this paper, the downlink is investigated for a point-to-multipoint HT-WBPLC indoor system. The sink is connected to a geolocation database to obtain the PU temporal and geographical map of access to the TV channels. Also, the noise is assumed to have zero mean and PSD N_0 .

A. Problem Formulation

In HT-WBPLC, there are N_1 subcarriers in HF band 1.8–30 MHz. In this band, HT-WBPLC transmitter uses the N_1 subcarriers of BPLC channel only under the PSD constraint of HomeplugAV2 [14]. In VHF band 30–200 MHz, there are N_2 subcarriers that are used by HT-WBPLC transmitter under one of the following two conditions.

- 1) *PU Absence*: In this case, HT-WBPLC transmitter uses both TVWS wireless channel and BPLC channel in the transmission of the data across the N_2 subcarriers. STBC is adopted in the transmission across the two channels in order to enhance the diversity gain. The transmission power is also constrained according to ECMA-392 standard in [19].
- 2) *PU Presence*: In this case, HT-WBPLC transmitter uses BPLC channel only in the transmission under the PSD constraint of HomeplugAV2. STBC is here adopted in the transmission across MIMO BPLC channels only.

Since we consider the case of downlink between the sink and the users, the target of the power and subcarrier allocation is to achieve maximum throughput and also satisfy different power constraints by different standards at different frequency bands. Let $P_{e_{nj}}$, $2^{k_{nj}}$, and P_{nj} be the BER, the constellation size and the allocated power for the n th subcarrier of the j th user, respectively, and N_t , N_r , and ζ be the numbers of Tx and Rx ports and STBC code rate, respectively. Let $h_{n_t n_r j}$ be the channel gain of spatial path $n_t n_r$ for a given subcarrier and user and $\alpha_{n_t n_r j}$ be the ratio of the power allocated at Tx for each spatial path. Following [38], $\alpha_{n_t n_r j}$ is calculated as:

$$\alpha_{n_t n_r j} = \sqrt{\frac{\beta_{n_t n_r j}}{\sum_{n_r=1}^{N_r} \beta_{n_t n_r j}}} \quad (1)$$

where $\beta_{n_t n_r j} = \sum_{n_r=1}^{N_r} |h_{n_t n_r j}|^2$. Let C_{nj} be the effective instantaneous MIMO channel gain for the n th subcarrier and the j th user after STBC decoder. C_{nj} can be calculated as $C_{nj} = \sum_{n_t=1}^{N_t} \alpha_{n_t n_r j} \sum_{n_r=1}^{N_r} |h_{n_t n_r j}|^2$. In the case of SISO channel, C_{nj} is simply the channel gain $|h_{n_t n_r j}|^2$ and $\alpha_{n_t n_r j}$ is taken as 1. Hence, a simple approximated probability of error expression can be adopted as in [39]

$$P_{e_{nj}} = \frac{0.2}{\left[1 + \frac{1.6 P_{nj} C_{nj}}{2^{k_{nj}} - 1 N_t \xi N_0}\right]^{N_t N_r}}. \quad (2)$$

Let the $P_{e_{nj}}$ be the same for all subcarriers and users and equal to the target probability of error P_e . Therefore, the number of bits k_{nj} assigned for subcarrier n and user j is expressed as

$$k_{nj} = \log_2 \frac{1 + 1.6 P_{nj} C_{nj}}{N_t \zeta N_0 \left[(0.2/P_e)^{\frac{1}{N_t N_r}} - 1 \right]}. \quad (3)$$

The second derivative of k_{nj} with respect to P_{nj} is negative, which proves that (3) is a concave function [40]. k_{nj} has three different expressions according to corresponding HT-WBPLC mode of operation.

1) *Mode A*: In this mode, BPLC channel is the only channel available and hence, N_{t_A} , N_{r_A} , and ζ are assumed to be equal to 1 for WBPLC. However, in HT-WBPLC, N_{t_A} and N_{r_A} are equal to 2. Also, the $P_{n_{AJ}}$ allocated to each subcarrier shall be lower than a maximum power P_A , which is the maximum power that can be allocated to the subcarrier to satisfy PSD constraint of HomeplugAV2 in HF band. The number of bits $k_{n_{AJ}}$ assigned to mode A subcarrier n_A of j th user can be expressed using (3) as

$$k_{n_{AJ}} = \log_2 \frac{1 + 1.6 P_{n_{AJ}} C_{n_{AJ}}}{N_{t_A} N_0 \left[(0.2/P_e)^{\frac{1}{N_{t_A} N_{r_A}}} - 1 \right]}. \quad (4)$$

2) *Mode B (30–84 MHz and PU Absence)*: In this case both BPLC and TVWS channels are used. Let PH_0 represent the probability of the PU absence. Since the frequency band from 30 to 54 MHz is not allowed for TVWS communication, PH_0 is equal to zero in this band. The number of bits $k_{n_{BJ}}^{(0)}$ assigned to mode B subcarrier n_B of the j th user can be expressed as

$$k_{n_{BJ}}^{(0)} = PH_0 \log_2 \frac{1 + 1.6 P_{n_{BJ}}^{(0)} C_{n_{BJ}}^{(0)}}{N_{t_B}^{(0)} N_0 \left[(0.2/P_e)^{\frac{1}{N_{t_B}^{(0)} N_{r_B}^{(0)}}} - 1 \right]}. \quad (5)$$

The allocated power $P_{n_{BJ}}^{(0)}$ for each subcarrier shall be below a maximum power $P_B^{(0)}$ to satisfy Tx power constraint of ECMA-392 standard. $N_{t_B}^{(0)}$ and $N_{r_B}^{(0)}$ take the value of 2 in case of WBPLC and the values of 2 and 3, respectively, in case of HT-WBPLC. ζ is taken as 1 for full rate STBC coding, where the superscript (0) indicates the absence of the PU.

3) *Mode C (30–84 MHz and PU Presence)*: In this case BPLC channel is the only channel used and hence, the $k_{n_{BJ}}^{(1)}$ can be expressed as

$$k_{n_{BJ}}^{(1)} = PH_1 \log_2 \frac{1 + 1.6 P_{n_{BJ}}^{(1)} C_{n_{BJ}}^{(1)}}{N_{t_B}^{(1)} (N_0 + N_p) \left[(0.2/P_e)^{\frac{1}{N_{t_B}^{(1)} N_{r_B}^{(1)}}} - 1 \right]} \quad (6)$$

where PH_1 and N_p represent PU presence probability and interference power, respectively. Also, the $P_{n_{BJ}}^{(1)}$ shall be below a certain power $P_B^{(1)}$ to satisfy PSD of HomeplugAV2 in VHF band. Let T be the overall throughput, which can be defined as

$$T = \Pi_{I0} (1 - P_e) \sum_{j=1}^K \left[\sum_{n_1=1}^{N_1} \frac{k_{n_{AJ}}}{t_1} + \frac{\sum_{n_B=1}^{N_2} (k_{n_{BJ}}^{(0)} + k_{n_{BJ}}^{(1)})}{t_2} \right] \quad (7)$$

where, Π_{I0} is the steady-state probability of nonburst impulsive state $I0$ of the BPLC channel [41]. T is considered as linear combination of k_{nj} , which is concave function with respect to P_{nj} . As a result, T is considered as concave function

with respect to P_{nj} . According to [40], maximizing a concave function is considered a convex optimization problem. Hence, the problem of maximizing overall throughput T can be expressed as

$$\begin{aligned} & \max_{P_{nAj}, P_{nBj}^{(0)}, P_{nBj}^{(1)}} T \\ \text{s.t. } & (C1) P_{nAj}, P_{nBj}^{(0)}, P_{nBj}^{(1)} \geq 0 \\ & (C2) \sum_{j=1}^K P_{nAj} \leq P_A \\ & (C3) \sum_{j=1}^K P_{nBj}^{(0)} \leq P_B^{(0)} \\ & (C4) \sum_{j=1}^K P_{nBj}^{(1)} \leq P_B^{(1)} \\ & (C5) \sum_{j=1}^K \left[\sum_{nA=1}^{N_1} P_{nAj} + \sum_{nB=1}^{N_2} PH_0 P_{nBj}^{(0)} \right. \\ & \quad \left. + PH_1 P_{nBj}^{(1)} \right] \leq P_{\text{in}} \\ & (C6) \frac{\sum_{nA=1}^{N_1} k_{nAj}}{t_1} + \frac{\sum_{nB=1}^{N_2} (k_{nBj}^{(0)} + k_{nBj}^{(1)})}{t_2} \geq R_j \end{aligned} \quad (8)$$

where N_1 and N_2 are the number of subcarriers in HF and VHF bands, respectively. Also, t_1 and t_2 are OFDM symbol durations in HomeplugAV2 and ECMA-392 standards, respectively. R_j is the throughput requested for each user. P_{in} is the total input power to the sink.

B. Problem Solution

The Lagrangian of the problem can be expressed as

$$\begin{aligned} L = & \Pi_{I0}(1 - P_e) \\ & \sum_{j=1}^K \left[\sum_{nA=1}^{N_1} \frac{1}{t_1} \log_2 \left\{ 1 + \frac{1.6P_{nAj} C_{nAj}}{N_0 \left[\left(\frac{0.2}{P_e} \right)^{\frac{1}{N_{fA} N_{rA}}} - 1 \right]} \right\} \right. \\ & \quad \left. + \sum_{nB=1}^{N_2} \frac{PH_0}{t_2} \log_2 \left\{ 1 + \frac{1.6P_{nBj}^{(0)} C_{nBj}^{(0)}}{\left(2N_0 \left[\left(\frac{0.2}{P_e} \right)^{\frac{1}{N_{fB}^{(0)} N_{rB}^{(0)}}} - 1 \right] \right)} \right\} \right. \\ & \quad \left. + \frac{PH_1}{t_2} \log_2 \left\{ 1 + \frac{1.6P_{nBj}^{(1)} C_{nBj}^{(1)}}{2(N_0 + N_p) \left[\left(\frac{0.2}{P_e} \right)^{\frac{1}{N_{fB}^{(1)} N_{rB}^{(1)}}} - 1 \right]} \right\} \right] \\ & - \lambda \sum_{j=1}^K \left[\sum_{nA=1}^{N_1} P_{nAj} + \sum_{nB=1}^{N_2} PH_0 P_{nBj}^{(0)} + PH_1 P_{nBj}^{(1)} \right] \\ & + \lambda P_{\text{in}} - \sum_{nA=1}^{N_1} \mu_{nA} \left[\sum_{j=1}^K P_{nAj} - P_A \right] \end{aligned}$$

$$\begin{aligned} & - \sum_{nB=1}^{N_2} \mu_{nB}^{(0)} \left[\sum_{j=1}^K P_{nBj}^{(0)} - P_B^{(0)} \right] \\ & - \sum_{nB=1}^{N_2} \mu_{nB}^{(1)} \left[\sum_{j=1}^K P_{nBj}^{(1)} - P_B^{(1)} \right] \\ & + \sum_{j=1}^K \beta_j \left[\sum_{nA=1}^{N_1} \frac{1}{t_1} \log_2 \left\{ 1 + \frac{1.6P_{nAj} C_{nAj}}{N_0 \left[\left(\frac{0.2}{P_e} \right)^{\frac{1}{N_{fA} N_{rA}}} - 1 \right]} \right\} \right. \\ & \quad \left. + \sum_{nB=1}^{N_2} \frac{PH_0}{t_2} \log_2 \left\{ 1 + \frac{1.6P_{nBj}^{(0)} C_{nBj}^{(0)}}{\left(2N_0 \left[\left(\frac{0.2}{P_e} \right)^{\frac{1}{N_{fB}^{(0)} N_{rB}^{(0)}}} - 1 \right] \right)} \right\} \right. \\ & \quad \left. + \frac{PH_1}{t_2} \log_2 \left\{ 1 + \frac{1.6P_{nBj}^{(1)} C_{nBj}^{(1)}}{2(N_0 + N_p) \left[\left(\frac{0.2}{P_e} \right)^{\frac{1}{N_{fB}^{(1)} N_{rB}^{(1)}}} - 1 \right]} \right\} \right] \\ & - \sum_{j=1}^K \beta_j R_j \end{aligned} \quad (9)$$

where, λ , μ_{nA} , $\mu_{nB}^{(0)}$, $\mu_{nB}^{(1)}$, and β_j are Lagrangian multipliers. Using the primal decomposition method, the problem in (9) can be divided into three convex optimization subproblems. Each subproblem is further decomposed into single variable convex optimization subproblems as function of the allocated power to each user and subcarrier as follows.

1) Subproblem 1:

$$L_1 = \Pi_{I0}(1 - P_e)$$

$$\begin{aligned} & \sum_{j=1}^K \sum_{nA=1}^{N_1} \frac{1 + \beta_j}{t_1} \log_2 \left\{ 1 + \frac{1.6P_{nAj} C_{nAj}}{N_0 \left[(0.2/P_e)^{\frac{1}{N_{fA} N_{rA}}} - 1 \right]} \right\} \\ & - \sum_{j=1}^K \sum_{nA=1}^{N_1} \lambda P_{nAj} - \sum_{nA=1}^{N_1} \sum_{j=1}^K \mu_{nA} \left[P_{nAj} - \frac{P_A}{K} \right]. \end{aligned} \quad (10)$$

The single variable convex subproblem is represented as

$$\begin{aligned} f_1(P_{nAj}) = & \Pi_{I0}(1 - P_e) \\ & \times \left[\frac{1 + \beta_j}{t_1} \log_2 \left\{ 1 + \frac{1.6P_{nAj} C_{nAj}}{N_0 \left[(0.2/P_e)^{\frac{1}{N_{fA} N_{rA}}} - 1 \right]} \right\} \right. \\ & \quad \left. - \lambda P_{nAj} - \mu_{nA} \left[P_{nAj} - \frac{P_A}{K} \right] \right]. \end{aligned} \quad (11)$$

2) Subproblem 2:

$$L_2 = \Pi_{I0}(1 - P_e) \sum_{j=1}^K \sum_{n_B=1}^{N_2} \frac{PH_0(1 + \beta_j)}{t_2} \\ \times \log_2 \left\{ 1 + \frac{1.6P_{n_B j}^{(0)} C_{n_B j}^{(0)}}{\left(2N_0 \left[\left(\frac{0.2}{P_e} \right)^{\frac{1}{N_{t_B}^{(0)} N_{r_B}^{(0)}}} - 1 \right] \right)} \right\} \\ - \sum_{j=1}^K \sum_{n_B=1}^{N_2} \lambda PH_0 P_{n_B j}^{(0)} - \sum_{n_B=1}^{N_2} \sum_{j=1}^K \mu_{n_B}^{(0)} \left[P_{n_B j}^{(0)} - \frac{P_B^{(0)}}{K} \right]. \quad (12)$$

The single variable convex subproblem is represented as

$$f_2(P_{n_B j}^{(0)}) = \Pi_{I0}(1 - P_e) \\ \left[\frac{PH_0(1 + \beta_j)}{t_2} \log_2 \left\{ 1 + \frac{1.6P_{n_B j}^{(0)} C_{n_B j}^{(0)}}{\left(2N_0 \left[\left(\frac{0.2}{P_e} \right)^{\frac{1}{N_{t_B}^{(0)} N_{r_B}^{(0)}}} - 1 \right] \right)} \right\} \right. \\ \left. - \lambda PH_0 P_{n_B j}^{(0)} - \left[P_{n_B j}^{(0)} - \frac{P_B^{(0)}}{K} \right] \right]. \quad (13)$$

3) Subproblem 3:

$$L_3 = \Pi_{I0}(1 - P_e) \sum_{j=1}^K \sum_{n_B=1}^{N_2} \frac{PH_1(1 + \beta_j)}{t_2} \\ \times \log_2 \left\{ 1 + \frac{1.6P_{n_B j}^{(1)} C_{n_B j}^{(1)}}{\left(2(N_0 + N_p) \left[\left(\frac{0.2}{P_e} \right)^{\frac{1}{N_{t_B}^{(1)} N_{r_B}^{(1)}}} - 1 \right] \right)} \right\} \\ - \sum_{j=1}^K \sum_{n_B=1}^{N_2} \lambda PH_1 P_{n_B j}^{(1)} - \sum_{n_B=1}^{N_2} \sum_{j=1}^K \mu_{n_B}^{(1)} \left[P_{n_B j}^{(1)} - \frac{P_B^{(1)}}{K} \right]. \quad (14)$$

The single variable convex subproblem is represented as

$$f_3(P_{n_B j}^{(1)}) \\ = \Pi_{I0}(1 - P_e) \left[\frac{PH_1(1 + \beta_j)}{t_2} \right. \\ \times \log_2 \left\{ 1 + \frac{1.6P_{n_B j}^{(1)} C_{n_B j}^{(1)}}{\left(2(N_0 + N_p) \left[\left(\frac{0.2}{P_e} \right)^{\frac{1}{N_{t_B}^{(1)} N_{r_B}^{(1)}}} - 1 \right] \right)} \right\} \\ \left. - \lambda PH_1 P_{n_B j}^{(1)} - \mu_{n_B}^{(1)} \left[P_{n_B j}^{(1)} - \frac{P_B^{(1)}}{K} \right] \right]. \quad (15)$$

After forming the Lagrangian functions and applying the Karush–Kuhn–Tucker conditions. The power allocated to each

mode of operation for subcarrier n and user j is expressed as

$$P_{n_A j} = \left[\frac{1 + \beta_j}{(t_1(\lambda + \mu_{n_A}))} - \frac{N_0 \left[\left(\frac{0.2}{P_e} \right)^{\frac{1}{(N_{t_A} N_{r_A})}} - 1 \right]}{1.6C_{n_A j}} \right] \quad (16)$$

$$P_{n_B j}^{(0)} = \left[\frac{PH_0(1 + \beta_j)}{(t_2(PH_0\lambda + \mu_{n_B}^{(0)}))} \right. \\ \left. - \frac{2N_0 \left[\left(\frac{0.2}{P_e} \right) \left(\frac{1}{(N_{t_B}^{(0)} N_{r_B}^{(0)})} \right) - 1 \right]}{1.6C_{n_B j}^{(0)}} \right] \quad (17)$$

$$P_{n_B j}^{(1)} = \left[\frac{PH_1(1 + \beta_j)}{(t_2(PH_1\lambda + \mu_{n_B}^{(1)}))} \right. \\ \left. - \frac{2(N_0 + N_p) \left[\left(\frac{0.2}{P_e} \right) \left(\frac{1}{(N_{t_B}^{(1)} N_{r_B}^{(1)})} \right) - 1 \right]}{1.6C_{n_B j}^{(1)}} \right]. \quad (18)$$

Using (16)–(18), the power and subcarriers are allocated for each user according to Algorithm 1

V. NUMERICAL RESULTS

In this section, the HT-WBPLC downlink model in Fig. 2 is used for simulation. The PU presence activity is represented using two-state discrete-time Markov chain model (DTMC), where the PU presence steady state probability for each 6 MHz TV channel is taken as 0.2. Also, impulsive noise is represented in our simulations by a two-state DTMC model, where the steady state probability of nonimpulsive state Π_{I0} is 0.9. The power line topology generator in [42] is used in the simulations to model the power line cable, terminal loads and outlet connection and hence, the power line channel. The topology generator in [42] is used to generate 100 topologies for each case of simulation and to calculate the average throughput. The VHF radio propagation channel is modeled as Rayleigh fading channel with average path loss as in [32]. In the simulations, HT-WBPLC is compared to MIMO BPLC [14] and TVWS systems. TVWS is implemented using ECMA-392 standard [19] and the FCC regulations [11].

A. HT-WBPLC Coverage

In Fig. 4, HT-WBPLC coverage distance is compared to those of 2×2 MIMO WiFi, TVWS, and MIMO BPLC communication systems. The achievable throughput by the proposed HT-WBPLC nearly doubles that achieved by MIMO BPLC. This proves the ability of our proposed system of improving both the coverage distance and throughput over other communication technologies.

Algorithm 1 Subcarrier and User Allocation

```

1: Initialization: Set  $\phi = \{1 \dots K\}$  as the set of users,  $\Omega_T = \{1 \dots N_1\} \cup \{1 \dots N_2\}$  as the set of all available subcarriers for all users.  $\Omega_j$  is the set of the subcarriers allocated to user  $j \in \phi$ ,  $\Omega_j = \{\phi\}$ .  $\beta_j, \mu_{n_A}, \mu_{n_B}^{(0)}, \mu_{n_B}^{(1)} = 0$ .
2: Allocate the maximum permissible power for each subcarrier  $P_{n_Aj} = P_A, P_{n_Bj}^{(0)} = P_B^{(0)}, P_{n_Bj}^{(1)} = P_B^{(1)}$ .
3: Start a For loop across the subcarriers of  $\Omega_T$ 
4: for  $k=1:N_1$  do
5:   Calculate  $k_{n_Aj}/t_1$  or  $(k_{n_Bj}^{(0)} + k_{n_Bj}^{(1)})/t_2$  for each user  $j$  in  $\phi$ .
6:   if  $k_{n_Aj}/t_1 > k_{n_A(j-1)}/t_1$  then
7:      $j \leftarrow n_A, \Omega_T = \Omega_T - n_A$ 
8:   else
9:     if  $(k_{n_Bj}^{(0)} + k_{n_Bj}^{(1)})/t_2 > (k_{n_B(j-1)}^{(0)} + k_{n_B(j-1)}^{(1)})/t_2$  then
10:     $j \leftarrow n_B, \Omega_T = \Omega_T - n_B$ 
11:   end if
12:   end if
13:   if  $R_j$  is achieved then
14:      $\phi = \phi - j$ 
15:   end if
16: end for
17: while sum of all transmission power is  $\leq P_{in}$  do
18:   Calculate the optimum power using the obtained user frequency map in the For loop with the aid of equations (16) - (18), and find the appropriate  $\lambda$  using the bisection method.
19:   if  $P_{n_Aj} > \mu_{n_A}$  then
20:      $P_{n_Aj} \leftarrow \mu_{n_A}$ 
21:   else
22:     if  $P_{n_Bj}^{(0,1)} > \mu_{n_B}$  then
23:        $P_{n_Bj}^{(0,1)} \leftarrow \mu_{n_B}$ 
24:     end if
25:   end if
26: end while

```

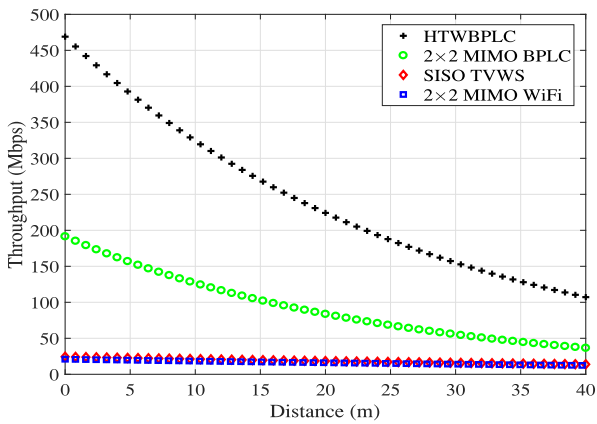


Fig. 4. Achievable throughput versus coverage distance.

Since the coverage area is considered as a main challenge for current indoor network technologies, a comparison between our proposed HT-WBPLC system and MIMO BPLC system is presented. In the comparison, a 500 m^2 area with

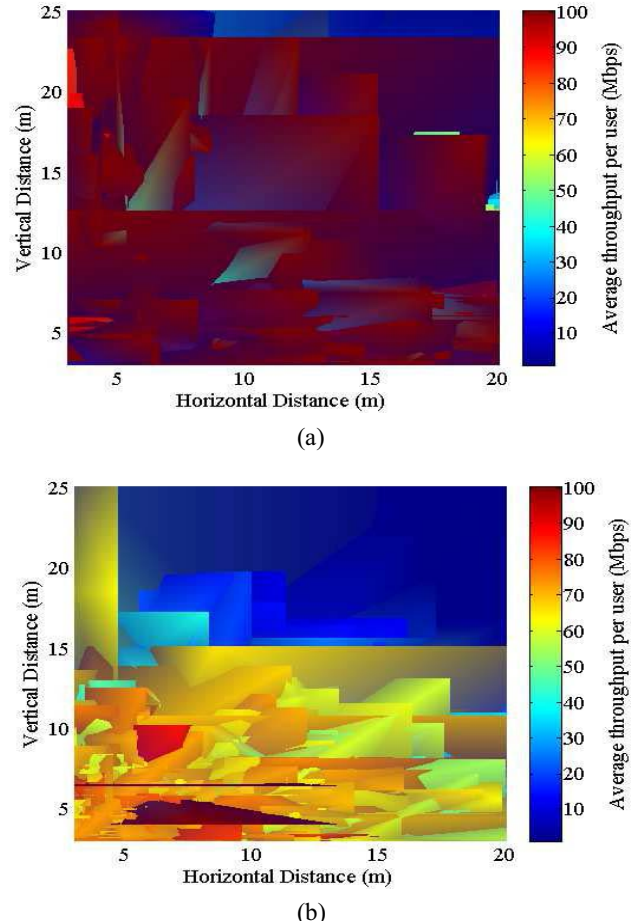


Fig. 5. Coverage heat map of (a) HT-WBPLC and (b) MIMO BPLC.

20 users is simulated for different BPLC topologies, load connections and users' distribution across the area. The average throughput for each user is calculated and compared against its location with respect to the sink location and hence, a coverage heat map is generated.

In Fig. 5(a) and (b) the coverage heat maps for HT-WBPLC and MIMO BPLC are presented, respectively. The areas which are covered by throughput $\leq 1 \text{ Mb/s}$ represent 20% of the total coverage area in MIMO BPLC case, compared to 15% in HT-WBPLC case. This shows the ability of HT-WBPLC to decrease the percentage of areas with limited coverage throughput. For coverage areas $\geq 400 \text{ m}^2$ the achieved average throughput per user offered by MIMO BPLC is 17 Mb/s , compared to 21.5 Mb/s offered by HT-WBPLC for each user. This shows the ability of HT-WBPLC system to increase the user throughput for large coverage areas by nearly 29% compared to MIMO BPLC.

B. HT-WBPLC Throughput

In Fig. 6, the throughput complementary cumulative distribution function (CCDF) of HT-WBPLC system is shown at different input power levels. The input power levels simulated are 50 mW, 100 mW, and 1 W, which are allocated in the downlink for different users and different subcarriers using Algorithm 1 in Section IV. For 50% of the time, HT-WBPLC

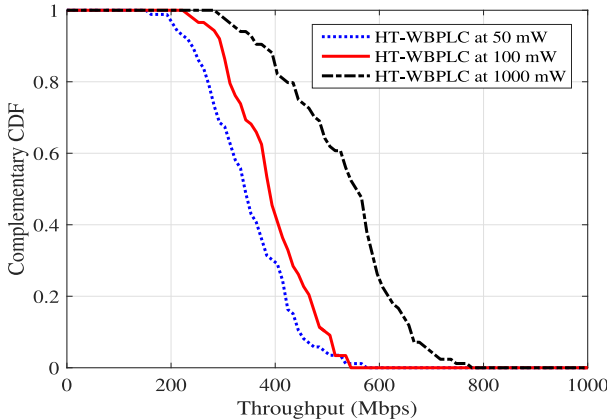


Fig. 6. Complementary CDF of the achievable throughput by the proposed HT-WBPLC using different input power levels.

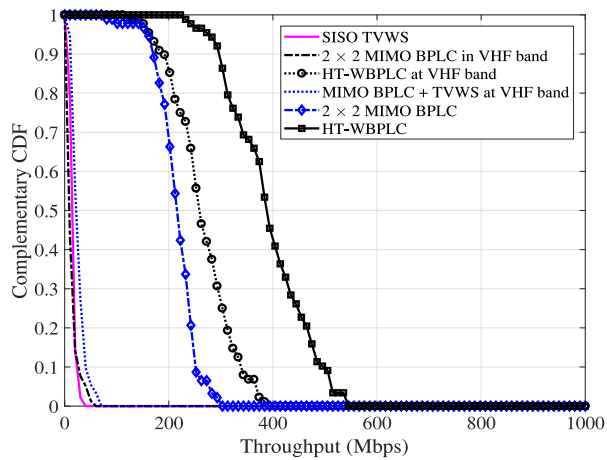


Fig. 7. Complementary CDF of the throughput using the proposed HT-WBPLC and the conventional MIMO BPLC.

achieves total downlink throughput of 565 and 343 Mb/s at input transmission power of 50 mW and 1000 mW, respectively. Therefore, an increase of 200 Mb/s is observed in the achievable throughput with the increase in the power level. Compared to MIMO BPLC [14], the proposed HT-WBPLC can support higher input power level as it complies with the requirements of the FCC regulations, which allow a 34 dB increase in the PSD than that allowed by HomeplugAV2 for BPLC.

In Fig. 7, our proposed HT-WBPLC is compared to MIMO BPLC in the frequency band 1.8–200 MHz at an input transmission power of 100 mW. The simulation results show that for 60% of the time, a throughput of 200 Mb/s is achieved using MIMO BPLC [14], while 380 Mb/s is achieved using HT-WBPLC which corresponds to 90% increase. Moreover, HT-WBPLC throughput CCDF is compared against MIMO BPLC [14] and TVWS in VHF band only. Significant throughput increase has been shown in VHF band by HT-WBPLC over the other two systems. This proves that the main reason behind the increase in the achievable throughput is due to VHF band exploitation. The increase is for two main reasons: 1) the addition of the wireless channel to the BPLC channel by adding a wireless VHF

antenna allows HT-WBPLC to be TVWS standard compliant, which results in higher permissible PSD and hence, higher throughput compared to HomeplugAV2 and 2) the increase in allowed spectrum of communication in VHF band up to 200 MHz.

VI. CONCLUSION

In this paper, an HT-WBPLC communication system has been proposed, which makes use of TVWS and BPLC channels in VHF bands cooperatively, based on the cognitive radio principle. HT-WBPLC benefits are twofold: 1) HT-WBPLC overcomes IoT network design challenge in realizing an integrated solution that incorporates BPLC and TVWS communication-based nodes, by offering a TVWS compliant perspective of BPLC standard and 2) HT-WBPLC also overcomes PSD constraints in BPLC and enables transmission in additional frequency band, and hence more coverage area. Our channel measurement results in Section III prove that the crosstalk channel between BPLC and TVWS can be exploited to enhance BPLC signal reception. Point-to-multipoint system simulation results have demonstrated that the proposed HT-WBPLC features a minimum of 40% over MIMO BPLC [14] and TVWS [11], [19], in term of total downlink throughput. Regarding network coverage, HT-WBPLC shows an increase in achievable user throughput by 29% compared to MIMO BPLC [14], for areas larger than or equal to 400 m². Therefore, HT-WBPLC is a promising solution for the growing needs of IoT.

REFERENCES

- [1] A. Al-Fuqaha, M. Guizani, M. Mohammadi, M. Aledhari, and M. Ayyash, "Internet of Things: A survey on enabling technologies, protocols, and applications," *IEEE Commun. Surveys Tuts.*, vol. 17, no. 4, pp. 2347–2376, 4th Quart., 2015.
- [2] L. Da Xu, W. He, and S. Li, "Internet of Things in industries: A survey," *IEEE Trans. Ind. Informat.*, vol. 10, no. 4, pp. 2233–2243, Jan. 2014.
- [3] K.-M. Kang and J. C. Park, "A new scheme for compliance with TV white space regulations using Wi-Fi modules in a cognitive radio system," *IEEE Trans. Consum. Electron.*, vol. 60, no. 4, pp. 567–573, Nov. 2014.
- [4] H. Wang, Y. Qian, and H. Sharif, "Multimedia communications over cognitive radio networks for smart grid applications," *IEEE Wireless Commun.*, vol. 20, no. 4, pp. 125–132, Aug. 2013.
- [5] M. U. Rehman *et al.*, "Achieving high data rate in multiband-OFDM UWB over power-line communication system," *IEEE Trans. Power Del.*, vol. 27, no. 3, pp. 1172–1177, Jul. 2012.
- [6] H. C. Ferreira, L. Lampe, J. Newbury, and T. Swart, Eds., *Power Line Communications: Theory and Applications for Narrowband and Broadband Communications Over Power Lines*. Chichester, U.K.: Wiley, 2010.
- [7] A. Ajiaz and A. H. Aghvami, "Cognitive machine-to-machine communications for Internet-of-Things: A protocol stack perspective," *IEEE Internet Things J.*, vol. 2, no. 2, pp. 103–112, Apr. 2015.
- [8] H.-C. Hsieh and C.-H. Lai, "Internet of Things architecture based on integrated PLC and 3G communication networks," in *Proc. IEEE 17th Int. Conf. Parallel Distrib. Syst. (ICPADS)*, Tainan, Taiwan, Dec. 2011, pp. 853–856.
- [9] C. Cano *et al.*, "State of the art in power line communications: From the applications to the medium," *IEEE J. Sel. Areas Commun.*, vol. 34, no. 7, pp. 1935–1952, Jul. 2016.
- [10] *Notice of Proposed Rule Making*, document 04-113, Federal Commun. Commision, Washington, DC, USA, May 2004.

- [11] *Second Report and Order and Memorandum Opinion and Order in the Matter of Unlicensed Operation in the TV Broadcast Bands, Additional Spectrum for Unlicensed Devices Below 900 MHz and in the 3 GHz Band*, document 08-260, Federal Commun. Commision, Washington, DC, USA, Nov. 2008.
- [12] M. Gebhardt, F. Weinmann, and K. Dostert, "Physical and regulatory constraints for communication over the power supply grid," *IEEE Commun. Mag.*, vol. 41, no. 5, pp. 84–90, May 2003.
- [13] T. Oliveira *et al.*, "Characterization of hybrid communication channel in indoor scenario," *J. Commun. Inf. Syst.*, vol. 31, no. 1, pp. 224–235, Sep. 2016.
- [14] L. T. Berger, A. Schwager, P. Pagani, and D. Schneider, *MIMO Power Line Communications: Narrow and Broadband Standards, EMC, and Advanced Processing*. Boca Raton, FL, USA: CRC Press, 2014.
- [15] P. Pagani *et al.*, "Electromagnetic compatibility for power line communications," in *Proc. IEEE 21st Int. Symp. Pers. Indoor Mobile Radio Commun. (PIMRC)*, Istanbul, Turkey, Sep. 2010, pp. 2799–2804.
- [16] T. Ronkainen, R. Vuohoniemi, and J.-P. Mäkelä, "Radiated interference of high frequency broadband power line communications," in *Proc. Int. Symp. Electromagn. Compat. (EMC Europe)*, Gothenburg, Sweden, Sep. 2014, pp. 555–559.
- [17] M. Heggo, X. Zhu, Y. Huang, and S. Sun, "A hybrid power line and TV white space MIMO system for indoor broadband communications," in *Proc. IEEE 84th Veh. Technol. Conf. (VTC-Fall)*, Montreal, QC, Canada, Sep. 2016, pp. 1–5.
- [18] M. Heggo, X. Zhu, S. Sumei, and Y. Huang, "White broadband power line communication: Exploiting the TVWS for indoor multimedia smart grid applications," *Int. J. Commun. Syst.*, vol. 30, no. 16, pp. 1–9, May 2017.
- [19] *MAC and PHY for Operation in TV White Space*, ECMA Standard ECMA-392, Dec. 2009.
- [20] Y. Zhang and C. Leung, "Resource allocation in an OFDM-based cognitive radio system," *IEEE Trans. Commun.*, vol. 57, no. 7, pp. 1928–1931, Jul. 2009.
- [21] H. Saki and M. Shikh-Bahaei, "Cross-layer resource allocation for video streaming over OFDMA cognitive radio networks," *IEEE Trans. Multimedia*, vol. 17, no. 3, pp. 333–345, Mar. 2015.
- [22] G. I. Tsipopoulos, O. A. Dobre, M. H. Ahmed, and K. E. Baddour, "Radio resource allocation techniques for efficient spectrum access in cognitive radio networks," *IEEE Commun. Surveys Tuts.*, vol. 18, no. 1, pp. 824–847, 1st Quart., 2016.
- [23] D. T. Ngo, C. Tellambura, and H. H. Nguyen, "Resource allocation for OFDMA-based cognitive radio multicast networks with primary user activity consideration," *IEEE Trans. Veh. Technol.*, vol. 59, no. 4, pp. 1668–1679, May 2010.
- [24] S. Zhang, W. Xu, S. Li, and J. Lin, "Resource allocation for multiple description coding multicast in OFDM-based cognitive radio systems with non-full buffer traffic," in *Proc. IEEE Wireless Commun. Netw. Conf. (WCNC)*, Shanghai, China, Apr. 2013, pp. 199–204.
- [25] K. Yang, W. Xu, S. Li, and J. Lin, "Distributed multicast resource allocation in OFDM-based cognitive radio networks," in *Proc. 8th Int. ICST Conf. Commun. Netw. China (CHINACOM)*, Guilin, China, Aug. 2013, pp. 57–62.
- [26] D. Makris, G. Gardikis, and A. Kourtis, "Quantifying TV white space capacity: Quantifying TV white space capacity," *IEEE Commun. Mag.*, vol. 50, no. 9, pp. 145–152, Sep. 2012.
- [27] D. Gurney, G. Buchwald, L. Ecklund, S. L. Kuffner, and J. Grosspietsch, "Geolocation database techniques for incumbent protection in the TV white space," in *Proc. 3rd IEEE Symp. New Front. Dyn. Spectr. Access Netw. (DYSPAN)*, McLean, VA, USA, Oct. 2008, pp. 1–9.
- [28] A. Achtzehn, J. Riihijärvi, and P. Mähönen, "Improving accuracy for TVWS geolocation databases: Results from measurement-driven estimation approaches," in *Proc. IEEE Int. Symp. Dyn. Spectr. Access Netw. (DYSPAN)*, McLean, VA, USA, Apr. 2014, pp. 392–403.
- [29] M. Heggo, X. Zhu, S. Sun, and Y. Huang, "A cognitive TV white space-broadband power line MIMO system for indoor communication networks," *J. Franklin Inst.*, vol. 355, no. 11, pp. 4755–4770, Jul. 2018.
- [30] N. Bounouader, S. Ghacham, G. Aniba, and Z. Guennoun, "Exploiting zero forcing beamforming and TV white space band for multiuser MIMO cognitive cooperative radio networks," in *Proc. Int. Conf. Wireless Netw. Mobile Commun. (WINCOM)*, Marrakech, Morocco, Oct. 2015, pp. 1–6.
- [31] M. Heggo, X. Zhu, Y. Huang, and S. Sun, "A novel statistical approach of path loss mapping for indoor broadband power line communications," in *Proc. IEEE Int. Conf. Smart Grid Commun. (SmartGridComm)*, Venice, Italy, Nov. 2014, pp. 499–504.
- [32] J. Andrusenko *et al.*, "VHF general urban path loss model for short range ground-to-ground communications," *IEEE Trans. Antennas Propag.*, vol. 56, no. 10, pp. 3302–3310, Oct. 2008.
- [33] W. A. Finamore, M. V. Ribeiro, and L. H.-J. Lampe, "Advancing power line communication: Cognitive, cooperative, and MIMO communication," in *Proc. Brazilian Telecommun. Symp.*, Brasília, Brazil, Sep. 2012, pp. 13–16.
- [34] P. Degauque, P. Laly, V. Degardin, M. Lienard, and L. Diquelou, "Compromising electromagnetic field radiated by in-house PLC lines," in *Proc. IEEE Glob. Telecommun. Conf. (GLOBECOM)*, Miami, FL, USA, Dec. 2010, pp. 1–5.
- [35] V. Degardin, P. Laly, M. Lienard, and P. Degauque, "Compromising radiated emission from a power line communication cable," *J. Commun. Softw. Syst.*, vol. 7, no. 1, pp. 16–21, Mar. 2011.
- [36] S. Chen, "Ultra wideband gigabit powerline communication," Ph.D. dissertation, School Electron. Eng. Comput. Sci., Queen Mary Univ. London, London, U.K., 2009.
- [37] A. M. Tonello and F. Versolatto, "Bottom-up statistical PLC channel modeling—Part II: Inferring the statistics," *IEEE Trans. Power Del.*, vol. 25, no. 4, pp. 2356–2363, Oct. 2010.
- [38] L. Xian and H. Liu, "An adaptive power allocation scheme for space-time block coded MIMO systems," in *Proc. IEEE Wireless Commun. Netw. Conf.*, New Orleans, LA, USA, Mar. 2005, pp. 504–508.
- [39] D. Wang, H. Minn, and N. Al-Dhahir, "A robust asynchronous multiuser STBC-OFDM transmission scheme for frequency-selective channels," *IEEE Trans. Wireless Commun.*, vol. 7, no. 10, pp. 3725–3731, Oct. 2008.
- [40] S. P. Boyd and L. Vandenberghe, *Convex Optimization*. Cambridge, U.K.: Cambridge Univ. Press, 2004.
- [41] J. Yin, X. Zhu, and Y. Huang, "Modeling of amplitude-correlated and occurrence-dependent impulsive noise for power line communication," in *Proc. IEEE Int. Conf. Commun. (ICC)*, Sydney, NSW, Australia, Jun. 2014, pp. 4565–4570.
- [42] A. M. Tonello and F. Versolatto, "Bottom-up statistical PLC channel modeling—Part I: Random topology model and efficient transfer function computation," *IEEE Trans. Power Del.*, vol. 26, no. 2, pp. 891–898, Apr. 2011.



Mohammad Heggo (S'08–M'17) received the B.Sc. and M.Sc. degrees in electrical engineering from Ain Shams University, Cairo, Egypt, in 2006 and 2010, respectively, and the Ph.D. degree in electrical engineering from the University of Liverpool, Liverpool, U.K., in 2017.

In 2007, he joined the Research and Development Department, Elsewedy Electrometer Company, 6th of October, Egypt, as an Embedded Communication Software Engineer. He is currently a Research Associate with the Electrical Engineering and Electronics Department, University of Manchester, Manchester, U.K. In 2013, he was awarded a dual Ph.D. scholarship for four years from the Electrical Engineering and Electronics, University of Liverpool and the Cognitive Communications Technology Department, Agency for Science, Technology, and Research, Singapore. His current research interests include power line communication, electromagnetic interference to transmission lines, cognitive radio, MIMO communication systems, and smart grid communications.



Sumei Sun (F'16) is currently the Head of the Communications and Networks Cluster and the Lead Principal Investigator of the Industrial Internet of Things Research Program with the Institute for Infocomm Research, Agency for Science, Technology, and Research, Singapore. Her current research interests include cognitive communications and networks, next-generation machine-type communications, and industrial Internet of Things.

Ms. Sun is serving as a member of the IEEE Communications Society Globecom/ICC Management and Strategy Standing Committee and the IEEE TRANSACTIONS ON WIRELESS COMMUNICATIONS Steering Committee, an Area Editor for the IEEE TRANSACTIONS ON VEHICULAR TECHNOLOGY, and an Editor for the IEEE COMMUNICATIONS SURVEYS AND TUTORIALS. She is a Distinguished Speaker of the IEEE Vehicular Technology Society from 2018 to 2021, the Vice Director of the IEEE Communications Society Asia-Pacific Board, and the Chapter Coordinator of the Asia-Pacific Region in the IEEE Vehicular Technologies Society.



Xu Zhu (S'02–M'03–SM'12) received the B.Eng. degree (with the First-Class Hons.) in electronics and information engineering from the Huazhong University of Science and Technology, Wuhan, China, in 1999, and the Ph.D. degree in electrical and electronic engineering from the Hong Kong University of Science and Technology, Hong Kong, in 2003.

She joined the Department of Electrical Engineering and Electronics, University of Liverpool, Liverpool, U.K., in 2003, where she is currently a Reader. She is also with the Harbin Institute of Technology, Shenzhen, China. She has over 160 peer-reviewed publications on communications and signal processing. Her current research interests include MIMO, channel equalization, resource allocation, cooperative communications, and green communications.

Dr. Zhu was an Editor for the IEEE TRANSACTIONS ON WIRELESS COMMUNICATIONS from 2012 to 2017 and a Guest Editor for a number of international journals such as *Electronics*. She has served as the Chair for various international conferences such as the Symposium Co-Chair of IEEE ICC 2016 and 2019, the Vice-Chair of the 2006 and 2008 ICARN International Workshops, the Program Chair of ICSAI 2012, and the Publicity Chair of IEEE IUCC-2016.



Yi Huang (S'91–M'96–SM'06) received the B.Sc. degree in physics from Wuhan University, Wuhan, China, in 1984, the M.Sc. (Engineering) degree in microwave engineering from the Nanjing Research Institute of Electronics Technology (NRIET), Nanjing, China, in 1987, and the D.Phil. degree in communications from the University of Oxford, Oxford, U.K., in 1994.

His experience includes three years spent with NRIET as a Radar Engineer and various periods with the University of Birmingham, Birmingham, U.K., the University of Oxford, Oxford, U.K., and the University of Essex, Colchester, U.K., as a member of Research Staff. He was a Research Fellow with British Telecom Labs, Martlesham, U.K., in 1994, and then joined the Department of Electrical Engineering and Electronics, the University of Liverpool, Liverpool, U.K., as a faculty member in 1995, where he is currently a Full Professor of wireless engineering, the Head of the High Frequency Engineering Group, and the Deputy Head of Department. He has authored or co-authored over 350 refereed papers in leading international journals and conference proceedings and has authored *Antennas: From Theory to Practice* (Wiley, 2008) and *Reverberation Chambers: Theory and Applications to EMC and Antenna Measurements* (Wiley, 2016). He has received many research grants from research councils, government agencies, charity, EU, and industry, acted as a consultant to various companies. His current research interests include wireless communications, applied electromagnetics, and radar and antennas.

Prof. Huang has served on a number of national and international technical committees and has been an Editor, an Associate Editor, or a Guest Editor of five international journals. He has been a Keynote/Invited Speaker and an Organizer of many conferences and workshops (e.g., WiCom 2006, 2010, IEEE iWAT2010, LAPC2012, and EuCAP2018). He is currently the Editor-in-Chief of *Wireless Engineering and Technology*, an Associate Editor of IEEE ANTENNAS AND WIRELESS PROPAGATION LETTERS, and the U.K. and Ireland Rep to the European Association of Antenna and Propagation, a Fellow of the IET, and a Senior Fellow of the HEA.